DOI: 10.1002/chem.201002944

Contiguous Metal-Mediated Base Pairs Comprising Two Ag^{I} Ions

Dominik A. Megger,[a] Célia Fonseca Guerra,[b] Jan Hoffmann,[c] Bernhard Brutschy,[c] F. Matthias Bickelhaupt,*[b] and Jens Müller*[a]

Dedicated to Professor Bernhard Lippert on the occasion of his 65th birthday

Abstract: The incorporation of transition-metal ions into nucleic acids by using metal-mediated base pairs has proved to be a promising strategy for the site-specific functionalization of these biomolecules. We report herein the formation of Ag^+-mediated Hoogsteen-type base pairs comprising 1,3-dideaza-2′-deoxyadenosine and thymidine. By defunctionalizing the Watson–Crick edge of adenine, the formation of regular base pairs is prohibited. The additional substitution of the N3 nitrogen atom of adenine by a methine moiety increases the basicity of the exocyclic amino group. Hence, 1,3-dideazaadenine and thymine are able to incorporate two Ag^+ ions into their Hoogsteen-type base pair (as compared with one Ag^+ ion in base pairs with 1-deazaadenine and thymine). We show by using a combination of experimental techniques (UV and circular dichroism (CD) spectroscopies, dynamic light scattering, and mass spectrometry) that this type of base pair is compatible with different sequence contexts and can be used contiguously in DNA double helices. The most stable duplexes were observed when using a sequence containing alternating purine and pyrimidine nucleosides. Dispersion-corrected density functional theory calculations have been performed to provide insight into the structure, formation and stabilization of the twofold metalated base pair. They revealed that the metal ions within a base pair are separated by an Ag···Ag distance of about 2.88 Å. The Ag–Ag interaction contributes some 16 kcal mol^{-1} to the overall stability of the doubly metal-mediated base pair, with the dominant contribution to the Ag–Ag bonding resulting from a donor–acceptor interaction between silver 4d-type and 4s orbitals. These Hoogsteen-type base pairs enable a higher functionalization of nucleic acids with metal ions than previously reported metal-mediated base pairs, thereby increasing the potential of DNA-based nanotechnology.

Keywords: bioinorganic chemistry · DNA · nucleobases · silver · supramolecular chemistry

Introduction

The incorporation of artificial base pairs into nucleic acid double helices represents a versatile method for the functionalization of these self-assembling biomolecules. The base pairing in these surrogates may still rely on hydrogen-bonding interactions, but with artificial nucleobases.[1] Moreover, numerous examples exist in which the base pairs are held together by hydrophobic interactions[2] or coordinative bonds to a central metal ion.[3] The latter example, that is, the generation of metal-mediated base pairs, represents a particularly interesting type of functionalization. It has been envisaged that by using this method, metal-based properties, such as redox chemistry, magnetism, conductivity, or catalytic activity, might be passed on to the modified nucleic acid.[3b,4] Hence, this method provides an opportunity to enhance the scope of DNA nanotechnology even further.

Almost all metal-mediated base pairs reported to date comprise two (either like or unlike) nucleobases coordinated to one central metal ion. Metal ions incorporated into DNA oligonucleotide double helices comprising such base pairs include Ag^+, Cu^{2+}, Mn^{3+}, Ni^{2+}, Fe^{2+}, and Hg^{2+}.[5–10] By carefully choosing the appropriate nucleosides, even two different metal ions (Cu^{2+} and Hg^{2+}) can be site-specifically inserted into a DNA duplex.[11] Likewise, one metal-mediated base pair created from 5-fluorouracil has recently been reported to contain two Ag^+ ions within just one base pair.[10b] In addition to DNA, metal-mediated base pairs have been successfully included in other nucleic acids and nucleic acid derivatives such as RNA,[12] PNA,[13] and

[a] Dr. D. A. Megger, Prof. Dr. J. Müller
Institute for Inorganic and Analytical Chemistry
University of Muenster
Corrensstr. 28/30, 48149 Münster (Germany)
Fax: (+49) 251-83-36007
E-mail: mueller.j@uni-muenster.de

[b] Dr. C. Fonseca Guerra, Prof. Dr. F. M. Bickelhaupt
Department of Theoretical Chemistry and
Amsterdam Center for Multiscale Modeling (ACMM)
Scheikundig Laboratorium der Vrije Universiteit
De Boelelaan 1083, 1081 HV Amsterdam (The Netherlands)
Fax: (+31) 20-59-87629
E-mail: f.m.bickelhaupt@vu.nl

[c] Dipl.-Phys. J. Hoffmann, Prof. Dr. B. Brutschy
Institut für Physikalische and Theoretische Chemie
Goethe-Universität Frankfurt
Max-von-Laue-Str. 7, 60438 Frankfurt (Germany)

Supporting information for this article is available on the WWW under http://dx.doi.org/10.1002/chem.201002944.

GNA.[9a,14] In total, three metal-containing duplexes of this type have been structurally characterized to date. The DNA structures differ significantly and appear to depend not only on the type of artificial base pair but also on the surrounding sequence of natural nucleobases. For example, the incorporation of two pyridine-2,6-dicarboxylate···Cu^{2+}···pyridine base pairs into a DNA sequence of alternating pyrimidine and purine bases resulted in the formation of a Z-DNA structure.[9d] In contrast, a DNA duplex comprising three contiguous imidazole···Ag^{+}···imidazole base pairs surrounded by natural A···T base pairs was shown to adopt a regular B-DNA conformation with only minor structural deviations.[5a] The structure adopted by a GNA duplex with hydroxypyridonate···Cu^{2+}···hydroxypyridonate base pairs is defined mainly by the acyclic backbone and appears to be only slightly influenced by the artificial base pair.[14]

The diversity of the duplex conformations observed to date for nucleic acids comprising metal-mediated base pairs is very promising with respect to the development of new base pairs of this type, because it shows a wide structural flexibility of the metal-modified nucleic acids. For example, we have recently shown that oligonucleotides comprising a natural pyrimidine nucleobase (namely thymine) and a purine-derived artificial nucleobase (namely 1-deazaadenine) can adopt a stable duplex structure in the presence of Ag^{+} ions.[5d] Geometrical considerations suggest that these Ag^{+}-mediated base pairs are of the Hoogsteen type. The development of additional metal-mediated Hoogsteen-type base pairs represents an interesting goal, particularly in the context of expanding the genetic code. Indeed, the natural nucleobases cytosine and guanine have already been shown to be able to engage in metal-mediated Hoogsteen base pairing.[15] However, no suitable artificial purine derivative has yet been established that selectively forms metal-mediated base pairs. Attempts to use cytosine in combination with 6-nitro-1,3-dideazapurine resulted only in the formation of Ag^{+}-mediated cytosine self pairs.[5b] Herein, we report on the use of 1,3-dideaza-2′-deoxyadenosine **5** (Scheme 1) as a nucleoside that is complementary to thymidine. This nucleoside has been obtained by a five-step synthesis in an overall yield of 32% (see the Experimental Section), which represents a major advancement compared with the rather tedious seven-step synthesis of the previously investigated 1-deaza-2′-deoxyadenosine by which the nucleoside was obtained in an overall yield of only 5%.[5d] In principle, both 1-deazaadenine and 1,3-dideazaadenine should form exclusively Hoogsteen base pairs because of the lack of an endocyclic hydrogen bond acceptor in the six-membered ring. However, different base-pairing properties have previously been reported in the absence of Ag^{+}. Whereas 1-deazaadenine forms stable Hoogsteen-type duplexes in the absence of Ag^{+},[16] 1,3-dideazaadenine does not do so despite an identical sequence.[17] It was therefore highly interesting to study 1,3-dideazaadenine in the context of metal-mediated base pairs and to investigate whether the different base-pairing properties would also be manifested in the presence of Ag^{+}.

Results and Discussion

Synthesis of 1,3-dideaza-2′-deoxyadenosine: The artificial nucleoside 1,3-dideaza-2′-deoxyadenosine **5** was synthesized from 2,6-dinitroaniline by a five-step synthesis. The first four steps were carried out according to literature procedures.[5b,18,19] The final reduction of **4** was achieved using Raney nickel with hydrazine hydrate in methanol (see the Supporting Information). Scheme 1 gives an overview of the synthetic procedure. To obtain a monomer suitable for automated DNA synthesis according to the phosphoramidite method, three additional steps were performed. The exocyclic amino group of **5** was FMOC-protected, and DMT and CEDIP groups were attached to the 5′- and 3′-OH groups, respectively.[17]

Based on compound **8**, two oligonucleotide sequences **I** and **II** were synthesized (Table 1). These sequences contain

Table 1. Oligonucleotide sequences used in this study.

Oligonucleotide	Sequence[a]
I	5′-d(XTX TXT XTX TXT XTX TXT)-3′
II	5′-d(XXX XXX XXX TTT TTT TTT)-3′

[a] X = 1,3-dideazaadenine, T = thymine.

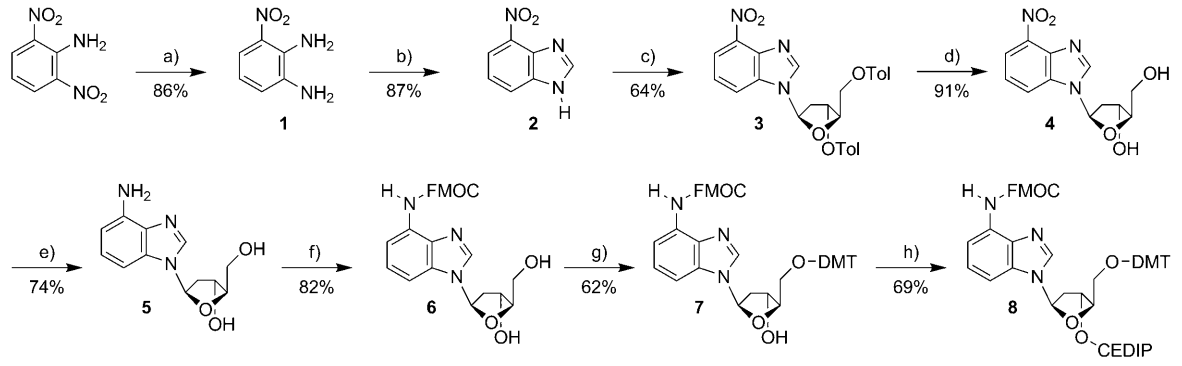

Scheme 1. Synthesis of 1,3-dideaza-2′-deoxyadenosine **5**. a) Na_2S, $NaHCO_3$, H_2O;[18] b) formic acid;[19] c) i) NaH, ii) Hoffer's chloro sugar, CH_3CN;[5b] d) NH_3 (aq), CH_3OH; e) Raney nickel, hydrazine hydrate, CH_3OH; f) TMS-Cl, FMOC-Cl, pyridine;[17] g) DMT-Cl, pyridine;[17] h) CEDIP-Cl, CH_2Cl_2.[17] FMOC = fluorenylmethoxycarbonyl, DMT = 4,4′-dimethoxytrityl, CEDIP = cyanoethyl-*N*,*N*-diisopropyl phosphoramidite.

exclusively 1,3-dideazaadenine (X) and thymine (T). Sequence **I** should be able to adopt either an antiparallel- or a parallel-stranded alignment. In the latter case, the duplex would contain single-nucleotide overhangs at the 5′- and 3′-ends. In contrast, sequence **II** is self-complementary only if an antiparallel-stranded duplex is formed. The Ag^+-binding behavior of oligonucleotides **I** and **II** was characterized by means of UV and circular dichroism (CD) spectroscopies, dynamic light scattering, and mass spectrometry.

UV melting curves: For oligonucleotide **I**, no cooperative melting was observed in the absence of Ag^+, which is in agreement with earlier reports.[17] However, distinct melting curves were obtained in the presence of Ag^+ (Figure 1a),

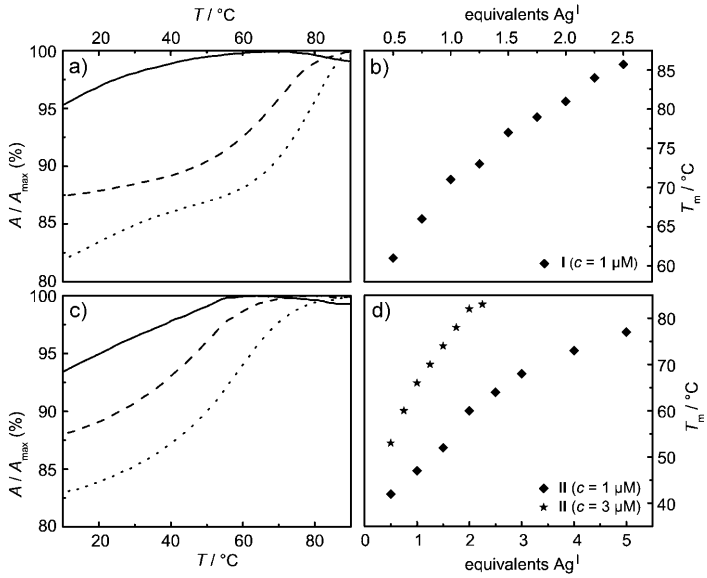

Figure 1. a) and c) UV melting curves of **I** and **II**, respectively, in the presence of various amounts of $AgNO_3$ (0 equiv (——), 1 equiv (– – –), 2 equiv (•••••)); b) and d) changes of T_m upon the addition of Ag^+. Conditions: 1 μM oligonucleotide, 150 mM $NaClO_4$, 5 mM MOPS (pH 6.8).

with the melting temperature T_m increasing smoothly upon the addition of $AgNO_3$ (Figure 1b). In the presence of two equivalents of Ag^+, the melting temperature of the duplex was 82 °C. In this context and throughout this discussion, one equivalent of metal ions corresponds to one metal ion per potential metal-mediated base pair. Therefore, in the case of an 18-mer oligonucleotide in which each base pair is mediated by one metal ion, one equivalent corresponds to 18 metal ions.

Similar observations were also made for oligonucleotide **II** (Figure 1c and d). T_m was seen to increase significantly up to the presence of about two equivalents of $AgNO_3$. Addition of more Ag^+ led to a slightly less steep increase in T_m. The melting temperatures of **II** in the presence of two equivalents of Ag^+ were 62 °C ($c = 1$ μM) and 83 °C ($c = 3$ μM). Based on this concentration dependence of T_m, the formation of a hairpin structure can be excluded, because the formation and dissociation of a hairpin are unimolecular and therefore concentration-independent processes. Compared with that of **I**, T_m is lower by 20 °C. This significant difference in duplex stability is in good agreement with the fact that Hoogsteen-type double helices are preferentially formed from alternating AT sequences.[20]

These UV melting studies of **I** and **II** are at variance with previous observations for 1-deazaadenine-containing oligonucleotides, for which T_m remained constant in the presence of excess Ag^+.[5d] However, a further increase of T_m upon the addition of excess metal salt is not unprecedented and has been observed for other metal-mediated base pairs.[5b,c]

UV titrations: Since the data presented in Figure 1 do not allow a clear determination of the number of Ag^+ ions bound per base pair, additional titrations were performed and monitored by UV spectroscopy. In the case of **I**, significant changes in the UV spectrum were observed upon the addition of Ag^+ (Figure 2a). As these changes occurred in a

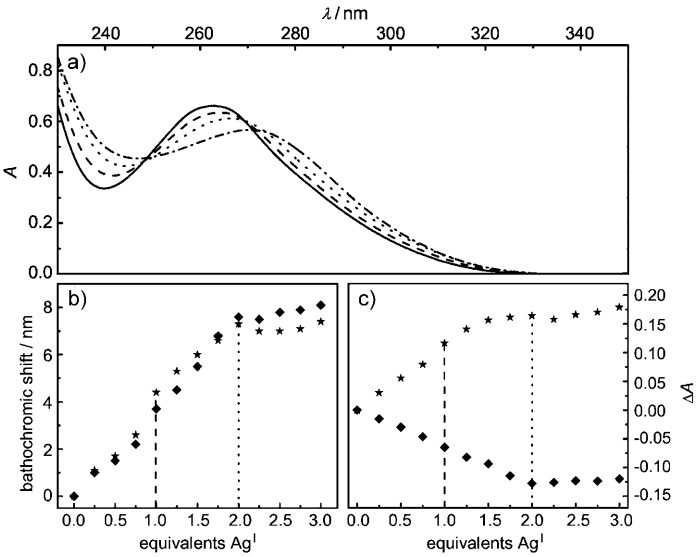

Figure 2. a) UV spectra of **I** in the presence of various amounts of $AgNO_3$ (0 equiv (——), 0.5 equiv (– – –), 1 equiv (•••••), 2 equiv (–•–•)); b) bathochromic shifts of the absorption minimum (originally at 240 nm (★)) and maximum (originally at 262 nm (◆)) of **I**; c) absorption changes at 240 (★) and 262 nm (◆), respectively, upon the addition of $AgNO_3$. In b) and c), one and two equivalents of Ag^+ are marked by broken and dotted lines, respectively. Conditions: 5 μM oligonucleotide, 150 mM $NaClO_4$, 5 mM MOPS (pH 6.8).

wavelength region in which the absorption is attributed to the nucleobases,[21] one can assume Ag^+ binding to these positions rather than the phosphate backbone. Plots of the absorption changes and of the bathochromic shifts of the absorption maximum and minimum clearly demonstrate major spectral changes upon the addition of the first two equivalents of Ag^+ (Figure 2b, c). Larger amounts of Ag^+ led to hardly any additional changes.

These results indicate that each metal-mediated base pair contains two Ag^+ ions. The second metal ion probably coor-

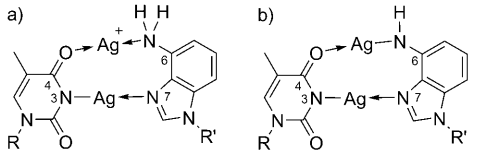

Scheme 2. Potential twofold-metalated base pairs between deprotonated thymine and a) 1,3-dideazaadenine or b) deprotonated 1,3-dideazaadenine (R, R′ = 2′-deoxyribose). Metal binding sites are numbered according to the purine and pyrimidine nomenclature.

dinates to the exocyclic functional groups of thymine and 1,3-dideazaadenine (Scheme 2). Such a twofold metalation might be facilitated by the fact that the free electron pair of the amino group of 1,3-dideazaadenine is not delocalized into the aromatic ring and can therefore act as a metal-binding site. Indeed, metalation of this site has been observed for the N9-methylated model nucleobase.[22]

Based on the experimental data, a two-step process for base-pair formation can be anticipated. Initially, base pairs mediated by a single Ag^+ are formed. Subsequently, a second, more weakly bound Ag^+ is inserted into each metal-mediated base pair. Such a mechanism is supported by DFT calculations (see below). Moreover, it is evidenced in the UV spectra by the observation that at certain wavelengths the coordination of the second metal ion results in less distinct spectral changes compared with the first one (Figure 2c, 240 nm). These different changes arise because coordination by the exocyclic groups of the nucleobases influences the electron-absorption spectrum to a different extent than coordination by endocyclic donor groups. Furthermore, the first metalation requires the deprotonation of thymine, which could contribute to the more significant changes observed upon the addition of the first equivalent of Ag^+. In principle, a neutral base pair (with the exocyclic amino group being deprotonated upon metalation) or a base pair with a single positive charge could be formed. However, formation of the former species appears less likely, as the exocyclic amino group of 1,3-dideazaadenine is expected to be relatively basic.[22] In fact, the pK_a values for protonations of N7 and N6 of 1,3-dideaza-2′-deoxyadenosine were determined by ^{1}H NMR spectroscopy to be 4.12 ± 0.03 and 0.8 ± 0.2, respectively (Figure S6 in the Supporting Information).

Similar observations were made in the case of oligonucleotide **II**. Here, however, the binding of the first and second Ag^+ ions per base pair resulted in slightly different changes in the UV spectrum. Comparably large changes were observed upon the addition of the first equivalent of Ag^+ (Figure S1a in the Supporting Information), whereas only minor but still significant changes were detectable upon the addition of the second equivalent (Figure S1b in the Supporting Information). Plots of the absorption changes and bathochromic shifts versus the equivalents of Ag^+ added showed the same results (Figure S1c and d in the Supporting Information). The less distinct changes in the UV spectra upon the addition of the second equivalent of Ag^+ can be attributed to the above-mentioned fact that Hoogsteen-type duplexes comprising alternating purine–pyrimidine sequences are particularly stable.[20] Hence, the duplex formed from sequence **I** probably adopted a slightly different conformation to that formed from sequence **II**. It is tempting to speculate that in the latter duplex the second Ag^+ ion is more exposed to the solvent and therefore dissociates more easily than in the duplex of oligonucleotide **I** (for further evidence, see the discussion of the mass spectra).

CD titrations: The oligonucleotides were investigated by CD spectroscopy to gather information on any conformational changes occurring during the Ag^+-mediated duplex formation. The CD spectrum of **I** displays two negative bands at 210 and 253 nm, as well as two positive ones at 227 and 280 nm. Upon the addition of Ag^+, the entire spectrum is redshifted (Figure 3a). Specifically, in the presence of two

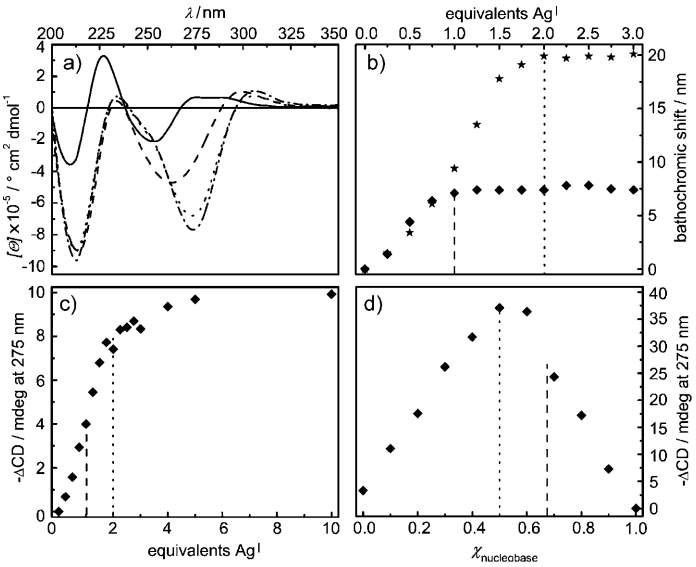

Figure 3. a) CD spectra of **I** in the presence of various amounts of $AgNO_3$ (0 equiv (——), 1 equiv (– – –), 2 equiv (•••••), 3 equiv (–•–•)); b) bathochromic shifts of the minimum originally at 252 nm (★) and the maximum originally at 227 nm (◆) upon the addition of Ag^+; c) change of the CD signal at 275 nm upon the addition of Ag^+; d) Job plot based on the CD signal at 275 nm, showing a 1:1 stoichiometry between nucleobases and Ag^+ ions (corresponding to two Ag^+ ions per base pair). For details regarding the Job plot, see the Experimental Section. In b)–d), one and two equivalents of Ag^+ per base pair are marked by broken and dotted lines, respectively. Conditions: 1 μM oligonucleotide (Job plot: 0.83–8.3 μM), 150 mM $NaClO_4$, 5 mM MOPS (pH 6.8).

equivalents of Ag^+, the minima are located at 212 and 275 nm, and the maxima at 233 and 306 nm. Interestingly, the positive band at 227 nm was only redshifted up to the addition of one equivalent of Ag^+, whereas the negative band at 252 nm shifted to longer wavelengths until two equivalents of Ag^+ had been added (Figure 3b). This is further evidence for a consecutive (rather than concomitant) incorporation of the two metal ions into the base pair. It is tempting to speculate that the changes at around 227 nm in-

dicate a conformational change from random coil to duplex upon the addition of the first equivalent of Ag^+. The second equivalent of Ag^+ mainly influences the base-pair structure, as indicated by the continuing spectral changes at around 252 nm. Upon the addition of more than two equivalents of Ag^+, only minor additional changes were observed (Figure 3c), confirming the proposed stoichiometry of the two-fold-metalated base pairs. Similar behavior was observed for oligonucleotide **II** (Figure S2 in the Supporting Information).

Job plots were generated to provide additional proof of the presence of two metal ions per base pair. Figure 3d shows the Job plot based on the CD signal at 275 nm. Additional Job plots (including those for oligonucleotide **II**) based on the bathochromic shifts in the CD spectrum and the UV spectrum are given in Figure S8 (in the Supporting Information). All of the Job plots clearly show a 1:1 stoichiometry (dotted line) between the nucleobases and the Ag^+ ions rather than a 2:1 stoichiometry (broken line). Hence, with one Ag^+ ion per nucleobase, two Ag^+ ions must be present per base pair, again indicating the formation of two-fold-metalated base pairs. It is interesting to note that the Job plot for oligonucleotide **II** shown in Figure S2d (in the Supporting Information) shows two points of discontinuity, corresponding to the incorporation of one and two Ag^+ ions per base pair, respectively. In good agreement with all of our other experiments, this suggests that in **II** the singly and doubly metalated base pairs are of similar stability, and hence that the second Ag^+ ion is weakly bound. For details regarding the generation of the Job plots, see the Experimental Section.

Dynamic light scattering: Dynamic light scattering (DLS) was used to further investigate the proposed formation of a double helix with metal-mediated base pairs. The results of the DLS measurements are given in Table 2. With a polydispersity not exceeding 30%, all samples were mono- to medium-disperse.

Table 2. Hydrodynamic radii r_H (nm) and polydispersities (%) of oligonucleotides **I** and **II** ($c = 0.3$ mM) in the presence of different equivalents of $AgNO_3$.[a]

Equiv of Ag^+	r_H [nm] (polydispersity)	
	I	**II**
0	1.4±0.1 (18)	1.4±0.1 (13)
1	2.0±0.2 (19)	1.8±0.1 (24)
2	6.6±1.4 (22)	5.4±1.1 (30)
5	6.4±1.4 (26)	5.6±0.5 (26)

[a] Values are the mean averages of at least five individual measurements. Error limits correspond to one standard deviation.

Within error limits of 3σ, the hydrodynamic radii of the oligonucleotides were identical in the absence and presence of the first equivalent of Ag^+. Nevertheless, when considering error limits of 1σ, the small increase of about 0.5 nm appears to become significant. It could be due to the formation of a double helix with metal-mediated base pairs incorporating only one Ag^+ per pair. To calculate theoretically the hydrodynamic radius for an 18-mer oligonucleotide duplex,[12] we assumed a helical rise of 0.34 nm and a helix diameter of 2 nm, both based on the ideal B-DNA geometry. Such an approximation is feasible because Hoogsteen-type double helices and B-DNA have very similar geometries.[20,23] The resulting theoretical value of 1.86 nm perfectly reproduced the experimentally determined radii of (2.0±0.2) and (1.8±0.1) nm, respectively. A significant increase in r_H was observed upon the addition of the second equivalent of Ag^+, whereas excess Ag^+ did not influence r_H any further. The large increase in r_H upon the addition of the second Ag^+ ion could be indicative of a change in the hydration of the DNA duplex.[24a] For example, the Ag^+ ions bound to the exocyclic groups of the nucleobases are expected to occupy some of the space formerly taken by hydrogen-bonded water molecules.[25] The release of structured water molecules upon the formation of a metal-mediated base pair has recently been reported for the thyminate···Hg^{2+}···thyminate base pair.[10a] A loose association of these water molecules would result in a larger apparent particle size.[24a] Moreover, whereas the first Ag^+ ion formally substitutes the thymine imino proton and hence does not change the overall charge of the base pair, the incorporation of the second Ag^+ ion is most probably not accompanied by deprotonation (see below). Hence, positive charge accumulates along the double helix, leading to the release of Na^+ ions. In analogy to the water molecules, the Na^+ ions are expected to remain in the vicinity of the oligonucleotide for electrostatic reasons, again providing a possible explanation for the increase in r_H. This suggestion is in agreement with previous observations that an accumulation of positive charge along the DNA helix leads to a significantly larger hydrodynamic radius.[24b]

Mass spectrometry: LILBID (laser-induced liquid bead ion desorption) mass spectrometric studies[26] were performed to finally prove the formation of metal-containing double helices. By virtue of its low consumption of analyte and soft laser-induced ion desorption, this recently developed technique is an adequate method for the investigation of biomolecules even in the presence of buffer.[27] In contrast to the UV, CD, and DLS experiments described above, in which only stoichiometric amounts of $AgNO_3$ were necessary to detect duplex formation, an excess of $AgNO_3$ (20 μM oligonucleotide and 1 mM $AgNO_3$) was applied during the incubation of the samples for analysis by mass spectrometry (for further details, see the Experimental Section).

Figure 4a shows LILBID mass spectra of oligonucleotide **I** recorded under soft conditions (i.e., with low laser power). They clearly verify that in the absence of Ag^+ no duplex was formed, since the major peak **A** corresponds to the single-stranded oligonucleotide ($m/z \approx 5.5$ kDa). In the presence of Ag^+, a different peak **C** was observed for the single-stranded oligonucleotide, shifted by about 0.7 kDa with respect to **A**. This peak can be assigned to a metalated single strand. Furthermore, a distinct peak **D** at $m/z \approx 13.7$ kDa appeared, corresponding to the mass of a metalated duplex

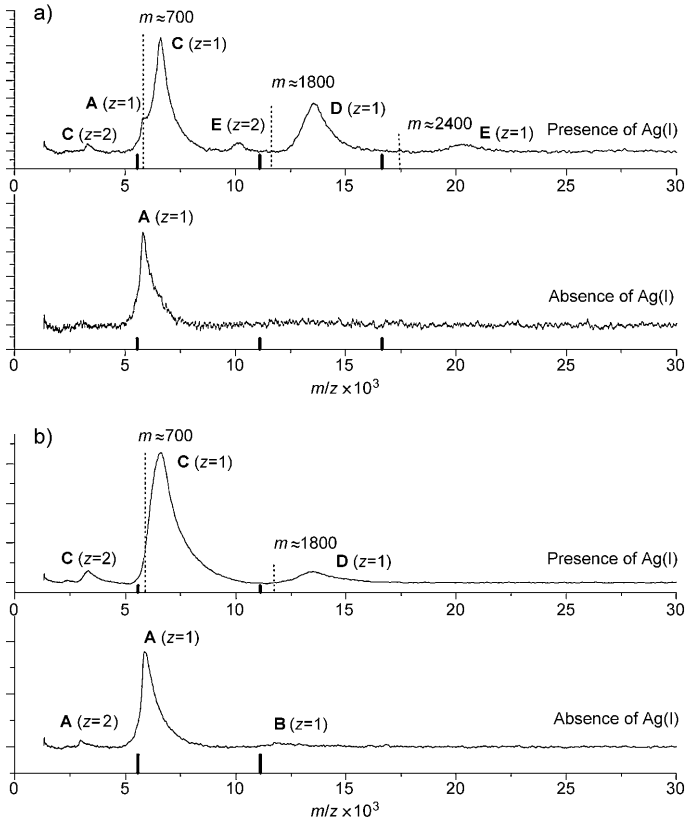

Figure 4. LILBID mass spectra of a) **I** and b) **II**. For an explanation of the letters **A**–**E**, see text. Black bars indicate the theoretically expected mass of the single strand and the resulting masses of hypothetical dimeric and trimeric aggregates, respectively. Dotted lines represent the peak maxima of the nonmetalated species used to determine the metal-induced mass shift. All spectra were recorded using the same laser energy.

($\Delta m \approx 1.8$ kDa compared with a hypothetical nonmetalated duplex). The mass shift Δm of about 1.8 kDa suggested that the duplex contained about 17 metal ions, corresponding to approximately one metal ion per base pair. For a duplex containing 18 twofold-metalated base pairs, a mass shift Δm of about 3.9 kDa would have been expected.

However, the metal ions coordinated by the exocyclic functional groups are less strongly bound than those coordinated by the endocyclic donor groups (see below for computational results). Hence, it is not necessarily surprising that they are not detectable under the experimental conditions. Surprisingly, a small peak **E** at $m/z \approx 20.2$ kDa appeared in the presence of Ag^+, which we tentatively assign to three oligonucleotide strands and 22 Ag^+ ions. The structure of the aggregate giving rise to this peak is not known. It might have formed as a result of the unusually high Ag^+ concentration used during sample preparation for the mass spectrometric studies. In fact, UV melting experiments on **I** in the presence of a large excess of Ag^+ also indicated the existence of an additional species (Figure S4 in the Supporting Information). The mass spectra of **II** (Figure 4b) are similar to those of **I**. A peak **A** for the single-stranded oligonucleotide was detected in the absence of Ag^+ ($m/z \approx 5.5$ kDa), accompanied by a much smaller peak **B** at $m/z \approx 12$ kDa, which we tentatively assign to an accidentally formed binary adduct of two single strands rather than a duplex. Moreover, metalated single strand **C** and double helix **D** were also observed in the presence of Ag^+. However, the ratio between the double and single strands was significantly lower compared with that gleaned from the mass spectrum of **I**. Further aggregation leading to higher aggregates was not apparent from the mass spectra of **II**. Spectra recorded at higher laser intensity, that is, under harsher conditions, indicated that the Ag^+–DNA adducts formed by **I** were more stable than those formed by **II**, as the former remained detectable, whereas in the case of the latter the Ag^+ ions were stripped off (Figure S3 in the Supporting Information). This observation is in good agreement with the higher stability of **I** indicated by the UV melting experiments. Moreover, a comparison of different laser energies in the case of **II** (Figure S3 in the Supporting Information) clearly showed that peak **D** indeed corresponded to a duplex based on metal-mediated base pairs. Upon removal of the Ag^+ ions by applying increased laser intensity, the duplex loses its structural integrity and dissociates into single strands rather than forming a nonmetalated duplex. Hence, the Ag^+ ions are an integral part of the double helix. In summary, even though the mass spectrometric studies do not resolve precisely how many Ag^+ ions are bonded to the oligonucleotide, they clearly verify that both **I** and **II** form double helices only in the presence of Ag^+.

DFT calculations: The Hoogsteen-type base pairs between thymine and 1,3-dideazaadenine were also examined from a theoretical point of view. In particular, dispersion-corrected DFT calculations were performed to determine whether a base pair containing one, two, or no metal ions is energetically favored. In total, four different base pairs were considered (Scheme 3).

The optimized geometries of the artificial base pairs **bp1**–**bp4** are shown in Figure 5. Each base pair displays an almost coplanar orientation of the nucleobases, apart from the gas-phase and solution structures of **bp3**. The increased distortion of **bp3** is most likely caused by the sp^3 hybridiza-

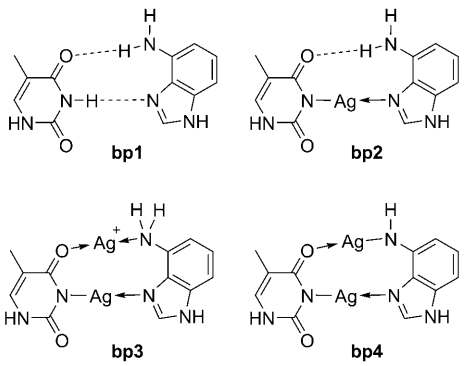

Scheme 3. Possible Hoogsteen-type base pairs between thymine and 1,3-dideazaadenine in the absence and presence of Ag^+.

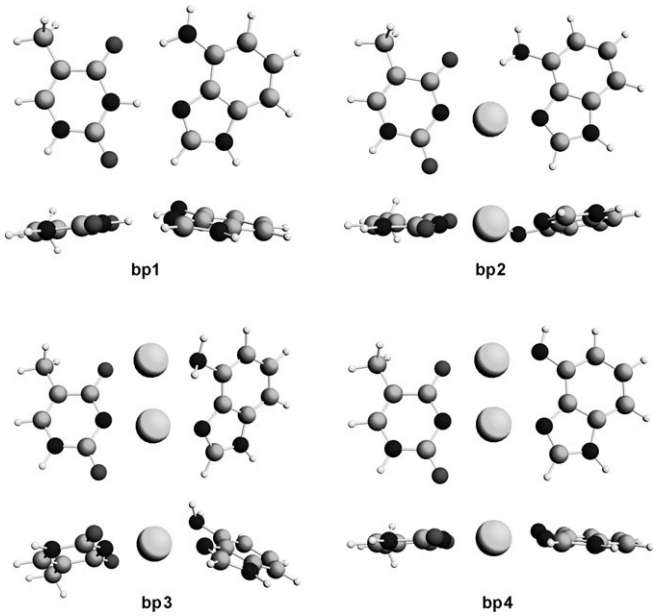

Figure 5. Top and side views of the geometry-optimized structures of **bp1**–**bp4** in water.

tion of the exocyclic amino group. Accordingly, **bp4** with an sp^2-hybridized amide as the metal-binding site is almost planar. Interestingly, those metal-mediated base pairs containing two metal ions display Ag···Ag distances of about 2.88 Å, far below the sum of their van der Waals radii (3.44 Å),[28] suggesting "argentophilic d^{10}–d^{10} interactions" between the Ag^+ ions.[29a] In fact, an even shorter Ag···Ag distance of 2.805(4) Å was previously observed by single-crystal X-ray diffraction analysis.[29b]

Argentophilic interactions are often accompanied by the emergence of fluorescent properties, although no definite correlation has yet been found between the presence or absence of closed-shell interactions and optical properties.[29a] In the presence of two equivalents of Ag^+, oligonucleotides **I** and **II** exhibit fluorescence at 475 and 454 nm, respectively, upon excitation at 270 nm (Figure S7 in the Supporting Information). In the absence of either Ag^+ or the oligonucleotides, no fluorescence is observed. Hence, the fluorescent properties support the presence of an argentophilic interaction as a result of the formation of metal-mediated base pairs, as suggested by the computational analysis.

We have investigated the nature of the interaction between the two silver centers in our base pair in more detail, by computing the interaction between the thyminate–Ag and dideazaadenine–Ag^+ fragments in the equilibrium structure **bp3** and in a deformed variant **bp3***, in which (proceeding from an otherwise frozen **bp3** structure) thymine was rotated by 90° about the N3–Ag axis and dideazaadenine by 180° about the Ag–N6 axis.[30] In the resulting **bp3*** structure (Figure S5 in the Supporting Information), the two N-Ag-N bridges no longer exist and the only contact between the thyminate–Ag and dideazaadenine–Ag^+ fragments is an Ag–Ag interaction. On going from **bp3** to **bp3***, the interaction between the two frozen fragments is weakened, from −83.7 to −16.2 kcal mol^{-1} (Table 3). This weakening reflects the interruption of the N-Ag-N bridges. This interruption is reflected by concomitant increases in the partial positive charges on the silver cations from +0.24 and +0.26 a.u. to +0.36 and 0.41 a.u., respectively, according to the VDD scheme (Table 4). Interestingly, however, the Ag–Ag interaction contributes some 16 kcal mol^{-1} to the overall stability of the doubly-metal-mediated base pair. As can be seen in Table 3, the Ag–Ag interaction in **bp3*** is little affected by switching off relativistic effects in the computations, which causes a weakening of only 1 kcal mol^{-1}. In comparison, in the base pair **bp3**, the N-Ag-N silver bridges are destabilized by a larger amount, namely 9 kcal mol^{-1}, if relativistic effects are not taken into account. We therefore conclude that the Ag–Ag interaction is not caused by an onset of relativistic effects.

Table 3. Bond analysis for **bp3** and **bp3***: energy decomposition analysis (in kcal mol^{-1}).[a]

	bp3		**bp3***	
ΔE_{Pauli}	150.2	(153.3)	21.2	(19.4)
ΔV_{elst}	−150.3	(−152.4)	−12.9	(−10.7)
ΔE_{oi}	−73.5	(−65.7)	−17.5	(−17.2)
ΔE_{disp}	−10.1	(−10.1)	−7.0	(−7.0)
ΔE_{int}	−83.7	(−74.9)	−16.2	(−15.3)

[a] Computed at the ZORA-BLYP-D/TZ2P//ZORA-BLYP-D/TZ2P level (in parentheses: non-relativistic values at BLYP-D/TZ2P//ZORA-BLYP-D/TZ2P). See Experimental Section for a description of the energy decomposition analysis (EDA).

Table 4. Bond analysis for **bp3** and **bp3***: VDD atomic charges (in a.u.) of Ag in the different fragments.[a]

	Separate fragments[b]	**bp3**	**bp3***
N3−Ag	0.407	0.240	0.357
N6−Ag^+	0.484	0.263	0.411

[a] Computed at the ZORA-BLYP-D/TZ2P//ZORA-BLYP-D/TZ2P level. [b] Separate fragments thyminate–Ag and dideazaadenine–Ag^+ as they occur in both **bp3** and **bp3***.

Further analyses of the orbital electronic structure in conjunction with energy decomposition analyses[31] showed that the dominant contribution to the Ag–Ag bonding in **bp3*** is a donor–acceptor interaction between occupied silver 4d-type orbitals and low-lying, empty 4s orbitals. Note that the orbital interaction component (−17.5 kcal mol^{-1}) is more stabilizing in **bp3*** than the electrostatic term (−12.9 kcal mol^{-1}). However, note also that the latter is still stabilizing, despite the partial positive charge on each silver center. This illustrates that point-charge models cannot be used to reproduce the electrostatic interaction as soon as the charge distributions of two fragments begin to overlap. The Ag–Ag donor–acceptor interactions do not substantially reduce the partial positive charges on the silver centers, which decrease from +0.41 and +0.48 a.u. in the separate fragments to +0.36 and +0.41 a.u., respectively, in **bp3***.

To determine which of these base pairs is formed preferentially, the reaction energies ΔE_{reac} for base-pair formation were calculated from the total bonding energies of the products E_P and the starting compounds of the base-pair formation E_S according to Equation (1).

$$\Delta E_{reac} = \Sigma E_P - \Sigma E_S \quad (1)$$

As can be seen from Figure 6a, the formation of the non-metalated base pair **bp1** is favored in the gas phase, because ΔE_{reac} amounts to $-16.0\,kcal\,mol^{-1}$. A metalation that requires the substitution of a proton by Ag^+ seems to be unfavorable, as shown by the highly positive ΔE_{reac} values for **bp2** and **bp4**. In contrast, the formation of the coordinative bonds O4–Ag and N6–Ag in **bp3** results in an energy gain of $-97.6\,kcal\,mol^{-1}$ compared with **bp2**. These data suggest that **bp1** will be preferentially formed in the gas phase. The results obtained in solution are in better agreement with the experimentally observed trends. Here, the non- and mono-metalated base pairs **bp1** and **bp2** are almost isoenergetic, with reaction energies of -8.9 and $-9.1\,kcal\,mol^{-1}$, respectively. Similar to the gas-phase situation, the incorporation of the second Ag^+ ion results in an energy gain (-33.2 kcal mol^{-1}). A subsequent deprotonation of the exocyclic amino group is unfavorable. Hence, in solution the formation of the twofold-metalated base pair **bp3** is favored.

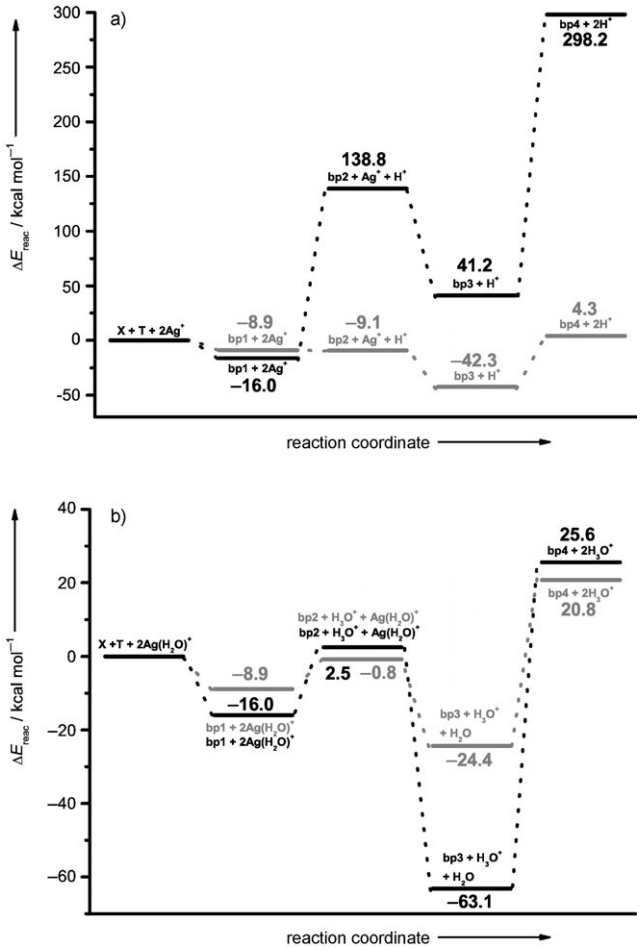

Figure 6. Energy diagrams showing a) the total reaction energies ΔE_{reac} ($kcal\,mol^{-1}$) for the formation of **bp1**–**bp4** in the gas phase (black) and in water (grey), and b) the corresponding ΔE_{reac} values ($kcal\,mol^{-1}$) obtained under consideration of microsolvation.

Additional calculations were performed considering microsolvation (Figure 6b). Here, the total bonding energies of geometry-optimized H_2O, $Ag(H_2O)^+$, and H_3O^+ were used during the calculations of ΔE_{reac} instead of Ag^+ and H^+. Such an inclusion of explicit water molecules that may act as either proton acceptors or aqua ligands is expected to describe the energetic devolution of the base-pair formation more precisely because, in this approach, the occurrence of charge transfer (donor–acceptor orbital) interactions between the solute and one of the solvent molecules is included explicitly. In fact, the experimentally observed trends are even reproduced in the gas phase by this calculation, since the formation of **bp3** ($\Delta E_{reac} = -63.1\,kcal\,mol^{-1}$) also becomes preferred. This stems from the fact that the substitution of the thymine imino proton by Ag^+, as occurs during the formation of **bp2**, is much less endothermic in solution than in the gas phase when microsolvation is not considered. Nonetheless, the deprotonation of the exocyclic amino group of 1,3-dideazaadenine, which is necessary for the formation of **bp4**, remains unfavorable. Similar trends were observed in solution, with the exception of the reaction energies of the twofold-metalated base pair **bp3**, which differ significantly. However, it is obvious that the inclusion of microsolvation is useful for the correct description of metal complexes with anionic ligands that are formed by the substitution of a proton by a metal ion.

To compare the overall stabilities of the artificial base pairs, the energies ΔE_{rel} relative to separate bases and silver cations were calculated according to Equation (2) from the total bonding energies of the base pairs E_{BP} and their respective monomeric subunits E_M. In the course of the calculations, the geometries of the monomeric subunits were also fully optimized.

$$\Delta E_{rel} = E_{BP} - \Sigma E_M \quad (2)$$

A comparison of ΔE_{rel} can be used to estimate the strength of the Ag^+–N interactions within the twofold-metalated base pair. Accordingly, the metal ion coordinated by N3 of thyminate and N7 of 1,3-dideazaadenine is bonded more strongly than the one coordinated by the exocyclic functional groups (Table 5). The increase in the overall base-pair stability resulting from the coordination of a

Table 5. Total interaction energies ΔE_{rel} ($kcal\,mol^{-1}$) of **bp2** and **bp3** in the gas phase and in water.

	ΔE_{rel}	
	bp2	**bp3**
gas phase	−215.0	−312.5
water	−55.5	−88.7

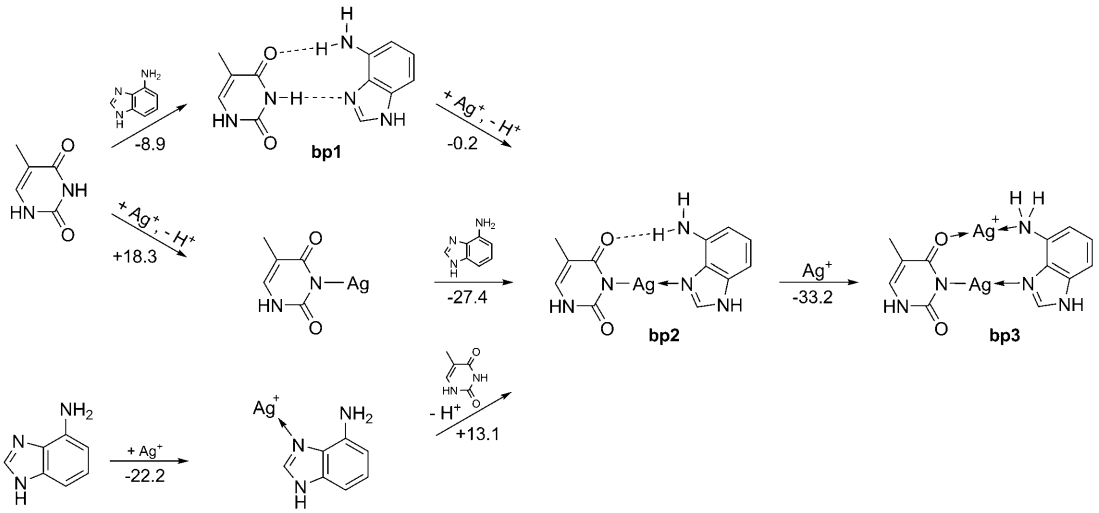

Scheme 4. Reaction paths of base-pair formation including the partial reaction energies $\Delta E_{reac(P)}$ (kcal mol^{-1}) in water.

second Ag^+ amounts to approximately one-half of that resulting from the coordination by N7 and N3. The higher stabilization in the case of the first Ag^+ is probably due to the fact that thyminate acts as an anionic ligand. These computational results are in good agreement with the mass spectrometric data, which suggest that one of the metal ions in the base pair is weakly bonded and therefore not detectable under the experimental conditions.

It should be noted that all of our calculations have been performed on the basis of individual base pairs. In the context of an entire DNA duplex, slightly different geometries might arise due to the more hydrophobic environment within a base pair stack. Moreover, the possibility that neighboring nucleosides might serve as additional ligands for the Ag^+ ions cannot be ruled out completely. Such a coordination pattern has previously been observed in the context of pyridine-2,6-dicarboxylate···Cu^{2+}···pyridine base pairs[9d] as well as in calculated structures of DNA duplexes comprising either hydroxypyridonate···Cu^{2+}···hydroxypyridonate base pairs or salen···Cu^{2+} base pairs.[32] In fact, the observations that oligonucleotide **I** forms significantly more stable duplexes than oligonucleotide **II** and that it binds the Ag^+ ions more tightly might be the result of such an additional coordination in the case of the alternating purine-pyrimidine sequence in **I**.

Mechanism of base-pair formation: To gain initial insight into the mechanistic details of the process of the formation of a metal-mediated base pair, the reaction energies ΔE_{reac} were divided into partial reaction energies $\Delta E_{reac(P)}$, which are calculated as the energy of the product relative to the energy of the preceding intermediate base pair (instead of relative to the separate monomeric subunits plus silver ions) as defined in Equation (3).

$$\Delta E_{reac(P)} = E_{BP} - E_{precedingBP} \quad (3)$$

A reaction scheme indicating $\Delta E_{reac(P)}$ of each reaction step is shown in Scheme 4. Three reaction paths are possible for the formation of **bp2**. One of these involves the initial formation of **bp1** and a concomitant metalation. In the other two cases, a metal complex of one of the nucleobases is formed prior to formation of the base pair. The latter two reaction paths seem to be unlikely, because the whole reaction is only exothermic along all elementary steps when it proceeds in water via **bp1**, with a $\Delta E_{reac(P)}$ of -8.9 and -0.2 kcal mol^{-1} for base pairing and metalation, respectively. In contrast, high-energy steps of $+18.3$ and $+13.1$ kcal mol^{-1} are expected if a metal complex with a single nucleobase is formed first. Hence, prior to the formation of a metalated base pair a nonmetalated one is probably formed, even though stable Hoogsteen-type duplexes of the nonmetalated type have not been observed experimentally.[17] However, the intermediate formation of a metalated nucleobase prior to base-pair formation cannot be ruled out completely, as both reaction pathways (i.e., via metalated thyminate or via metalated 1,3-dideazaadenine) involve reaction steps with a highly negative $\Delta E_{reac(P)}$ (-27.4 and -22.2 kcal mol^{-1}, respectively).

Conclusion

The oligonucleotides $d(XT)_9$ (**I**) and $d(X_9T_9)$ (**II**), containing 1,3-dideazaadenine, have been found to form stable double helices in the presence of Ag^+. Duplex formation has been confirmed by LILBID mass spectrometry, UV and CD spectroscopies, as well as dynamic light scattering. Most interestingly, the data indicate the formation of a base pair containing two metal ions. This is in contrast to previous experiments with 1-deazaadenine, which only binds one Ag^+ per metal-mediated base pair with deprotonated thymine,[5d] and is most likely attributable to the increased basicity of the exocyclic amino group in 1,3-dideazaadenine. Dispersion-

corrected DFT calculations have corroborated these experimental findings, revealing the favored formation of a two-fold-metalated base pair bearing one single positive charge. Bond analyses have indicated a substantial "argentophilic" Ag-d^{10}–Ag-d^{10} interaction of about 16 kcal mol^{-1} caused by charge transfer from silver 4d to 4s orbitals, which contributes to the stability of doubly metal-mediated base pairs such as **bp3**.

The observations presented herein allow important conclusions to be drawn regarding the generation and use of metal-mediated base pairs in the context of nucleic acid functionalization. 1) Subtle changes of a nucleobase involved in metal-mediated base pairing may have far-reaching consequences with respect to the metal-binding properties. 2) The oligonucleotide sequence can also play a significant role in determining the stability of the metal-mediated base pair. 3) The possibility of incorporating two metal ions into one base pair represents a significant step forward towards obtaining highly functionalized nucleic acids. 4) Mechanistic insights gained from calculations suggest that the metal ions are inserted in one of the late steps of base-pair formation. Interestingly, even though Hoogsteen duplexes comprising nonmetalated 1,3-dideazaadenine–thymine base pairs are not stable, this base pair might still be involved as an intermediate during the formation of its Ag^+-mediated analogue.

Experimental Section

1,3-Dideaza-2′-deoxyadenosine **5** and its FMOC-, DMT-, and CEDIP-protected analogue **8** were synthesized according to (partially modified) previously published procedures.[5b,17–19] DNA syntheses were performed in the DMT-off mode on a K&A Laborgeräte H8 DNA/RNA synthesizer following standard protocols (except for a threefold increase in coupling time for the artificial phosphoramidite). The oligonucleotides were cleaved from the solid support and deprotected by exposing them to *tert*-butylamine/methanol/water (1:2:1) for 3 h at 65 °C. They were purified by polyacrylamide gel electrophoresis under denaturating conditions (gel solution: 7 M urea, 1 M TBE buffer; 8–18% polyacrylamide/bisacrylamide (29:1); loading buffer: 11.8 M urea; 42 mM Tris·HCl, pH 7.5; 0.83 mM EDTA, pH 8.0; 8% sucrose). After purification, the oligonucleotides were desalted by passage through NAP 10 columns. The desalted oligonucleotides were identified by MALDI-TOF mass spectrometry (**I**: calcd for $[M+H]^+$: 5475 Da; found: 5476 Da; **II**: calcd for $[M+H]^+$: 5475 Da; found: 5474 Da). MALDI-TOF mass spectra were recorded on a Bruker Reflex IV instrument using a 3-hydroxypicolinic acid/ammonium citrate matrix. During quantification of the oligonucleotides, a molar extinction coefficient $\varepsilon_{260}=7.5$ cm^2 μmol^{-1} was used for **5**.

UV/Vis spectra were recorded on a Varian CARY BIO 100 spectrophotometer. CD spectra were recorded at 10 °C on a Jasco J-815 spectrometer. UV melting curves were recorded at 260 nm with a heating rate of 1 K min^{-1} and a data interval of 0.2 K. Melting temperatures were determined as the maxima of the first derivatives of the melting curves. Prior to each measurement, the samples were equilibrated by heating to 90 °C and then slowly cooling to 10 °C (cooling rate: 0.5 K min^{-1}).

For the generation of a Job plot, the sum of the molar fractions of both components needs to be constant during all measurements. When using a double helix (with 18 base pairs) as one component and an Ag^+ ion as the other component, a 1:18 stoichiometry (one Ag^+ ion per base pair) would have to be distinguished from a 1:36 stoichiometry (two Ag^+ ions per base pair). As it would be almost impossible to differentiate unambiguously a 0.06 ratio from a 0.11 ratio, a different approach has been used to obtain interpretable Job plots. Instead of defining one duplex as one of the components, we have defined one nucleobase as this component. Hence, a 1:1 stoichiometry in the Job plot (one Ag^+ ion per nucleobase) corresponds to two Ag^+ ions per base pair. Accordingly, the incorporation of only one Ag^+ ion per base pair would be represented by a 2:1 stoichiometry in the Job plot (two nucleobases per Ag^+ corresponding to one Ag^+ per base pair). For example, for the Job plot shown in Figure 3d, the total concentration was 150 μM. Hence, at $\chi_{nucleobase}=1$, the nucleobase concentration was 150 μM (corresponding to 8.3 μM oligonucleotide single strand or 4.2 μM double helix). Accordingly, at $\chi_{nucleobase}=0.1$, the nucleobase concentration was 15 μM (corresponding to 0.83 μM oligonucleotide single strand or 0.42 μM double helix), and the Ag^+ concentration was 135 μM.

DLS experiments were performed on a DynaPro Titan instrument from Wyatt Technology. The oligonucleotide samples ($c=0.3$ mM, 150 mM $NaClO_4$, 5 mM MOPS, pH 6.8) were incubated in the presence of the respective amounts of $AgNO_3$ by heating to 90 °C and then slowly cooled to 10 °C (cooling rate: 0.5 K min^{-1}). The samples were then centrifuged at 13500 rpm for at least 2 h. The supernatant was transferred to a 12 μL cuvette and measured.

LILBID experiments were performed on an in-house-constructed time-of-flight mass spectrometer (TOF-MS) of the Wiley–McLaren type. Details of this method have been published previously.[33] Briefly, the ion source contains a commercial droplet dispenser (Microdrop), which injects on demand tiny micro droplets (Ø ≈ 50 μm; V ≈ 65 pL) from 300 Torr through a pressure-reduction aperture into high vacuum (10^{-6} Torr). There, they are individually irradiated by high-intensity mid-IR laser pulses (λ ≈ 3 μm) generated by an in-house-constructed Nd:YAG-pumped $LiNbO_3$ optical parametric oscillator. Due to the absorption of the laser light by the solvent, beyond a certain intensity threshold the droplets are disrupted, ejecting preformed analyte ions into the vacuum. For the LILBID MS experiments, oligonucleotide samples (20 μM oligonucleotide, 0 or 1 mM $AgNO_3$ in 100 mM NH_4HCO_3/1 mM $Mg(NO_3)_2$, pH 7.4) were incubated at 30 °C overnight, followed by a buffer exchange to 20 mM NH_4HCO_3/1 mM $Mg(NO_3)_2$, pH 7.4.

All calculations were performed using dispersion-corrected density functional theory (DFT-D) as implemented in the Amsterdam Density Functional program (ADF 2009.1).[34] Geometry optimizations were performed using analytical gradient techniques and without any symmetry or geometrical constraints. All geometries were verified as true energy minima, having no imaginary frequencies, by means of vibrational analyses. The dispersion-corrected GGA functional BLYP-D,[35] which has proved to be adequate for calculations of DNA base dimers,[36] was used with the doubly polarized, triple-ζ-quality basis set TZ2P.[37]

In BLYP-D, the BLYP functional[35c,d] is augmented with an empirical correction for long-range dispersion effects, described by a sum of damped interatomic potentials of the form C_6R^{-6} added to the usual DFT energy.[35a,d] The TZ2P basis set used herein is a large uncontracted set of Slater-type orbitals (STOs) containing diffuse functions (no Gaussian functions are involved).[34] The basis set is of triple-ζ quality for all atoms and is augmented with two sets of polarization functions, that is, 3d and 4f on C, N, O and 2p, 3d on H. The 1s core shells of C, N, and O were treated by the frozen-core approximation. An auxiliary set of s, p, d, f, and g STOs was used to fit the molecular density and to accurately represent the Coulomb and exchange potentials in each self-consistent field cycle. The basis set superposition error (BSSE) in the bond energy has previously been shown to be only 1 kcal mol^{-1} or less in GGA calculations involving the TZ2P basis set. Moreover, the dispersion correction in the present calculations has been developed such that these small BSSE effects are absorbed into the empirical potential.[35a] Therefore, no explicit counterpoise corrections had to be carried out. In addition, scalar relativistic effects were taken into account by using the zeroth-order regulator approximation (ZORA).[38]

For calculations in water, solvent effects were estimated using the conductor-like screening model (COSMO).[39] In the COSMO calculations, a corrected ion radius of Ag^+ and a corrected solvation energy of H^+ were used. Parameterization was accomplished by performing a series of

single-point calculations on Ag^+ using COSMO with different radii. The radius resulting in a solvation energy that matched the experimentally observed value was subsequently chosen for all COSMO calculations ($\Delta G_{solv}(exp) = -102.8$ kcal mol^{-1};[40] $\Delta G_{solv}(calcd) = -102.6$ kcal mol^{-1} for $r = 1.670$ Å). For isolated H^+, the experimental solvation energy (-250.8 kcal mol^{-1})[40] was used directly in the evaluation of the corrected total bonding energy.

Analyses of the base-pairing interactions were carried out in the framework of Kohn–Sham DFT using the Kohn–Sham molecular orbital (MO) model in conjunction with a quantitative energy decomposition analysis (EDA).[30,31a] The interaction energy is decomposed into four physically meaningful terms: $\Delta E_{int} = \Delta V_{elst} + \Delta E_{Pauli} + \Delta E_{oi} + \Delta E_{disp}$. The term ΔV_{elst} corresponds to the classical electrostatic interaction between the unperturbed charge distributions of the deformed bases and is usually attractive. The Pauli repulsion ΔE_{Pauli} comprises the destabilizing interactions between occupied orbitals and is associated with steric repulsion. The orbital interaction ΔE_{oi} accounts for charge transfer and polarization. The term ΔE_{disp} accounts for the long-range dispersion effects. For a more detailed explanation of the energy terms, see references [30,31a].

Acknowledgements

Generous financial support by the Deutsche Forschungsgemeinschaft (MU 1750/2–1, IRTG 1444), the National Research School Combination–Catalysis (NRSC-C), and the Netherlands Organization for Scientific Research (NWO-CW and NWO-NCF) is gratefully acknowledged. BB acknowledges the support of the Cluster of Excellence Frankfurt (CEF) "Macromolecular Complexes" and of the Centre for Membrane Proteomics (CMP). The authors thank Eva Freisinger for access to the DLS instrument and Nicole Megger for performing the DLS measurements. We thank Luisa De Cola for access to the fluorescence spectrophotometer and Cristian Strassert for assisting in the fluorescence measurements.

[1] a) S. A. Benner, *Acc. Chem. Res.* **2004**, *37*, 784–797; b) A. T. Krueger, H. Lu, A. H. F. Lee, E. T. Kool, *Acc. Chem. Res.* **2007**, *40*, 141–150.

[2] a) E. T. Kool, H. O. Sintim, *Chem. Commun.* **2006**, 3665–3675; b) Z. Johar, A. Zahn, C. J. Leumann, B. Jaun, *Chem. Eur. J.* **2008**, *14*, 1080–1086.

[3] a) J. Müller, *Eur. J. Inorg. Chem.* **2008**, 3749–3763; b) G. H. Clever, M. Shionoya, *Coord. Chem. Rev.* **2010**, *254*, 2391–2402; c) G. H. Clever, C. Kaul, T. Carell, *Angew. Chem.* **2007**, *119*, 6340–6350; *Angew. Chem. Int. Ed.* **2007**, *46*, 6226–6236; d) K. Tanaka, M. Shionoya, *Coord. Chem. Rev.* **2007**, *251*, 2732–2742; e) W. He, R. M. Franzini, C. Achim, *Prog. Inorg. Chem.* **2007**, *55*, 545–611.

[4] a) J. Müller, *Nature* **2006**, *444*, 698; b) T. Carell, C. Behrens, J. Gierlich, *Org. Biomol. Chem.* **2003**, *1*, 2221–2228.

[5] a) S. Johannsen, N. Megger, D. Böhme, R. K. O. Sigel, J. Müller, *Nat. Chem.* **2010**, *2*, 229–234; b) D. A. Megger, J. Müller, *Nucleosides Nucleotides Nucleic Acids* **2010**, *29*, 27–38; c) D. Böhme, N. Düpre, D. A. Megger, J. Müller, *Inorg. Chem.* **2007**, *46*, 10114–10119; d) F.-A. Polonius, J. Müller, *Angew. Chem.* **2007**, *119*, 5698–5701; *Angew. Chem. Int. Ed.* **2007**, *46*, 5602–5604; e) J. Müller, D. Böhme, P. Lax, M. Morell Cerdà, M. Roitzsch, *Chem. Eur. J.* **2005**, *11*, 6246–6253.

[6] a) Y. Takezawa, K. Tanaka, M. Yori, S. Tashiro, M. Shiro, M. Shionoya, *J. Org. Chem.* **2008**, *73*, 6092–6098; b) K. Tanaka, A. Tengeiji, T. Kato, N. Toyama, M. Shionoya, *Science* **2003**, *299*, 1212–1213; c) K. Tanaka, Y. Yamada, M. Shionoya, *J. Am. Chem. Soc.* **2002**, *124*, 8802–8803; d) K. Tanaka, A. Tengeiji, T. Kato, N. Toyama, M. Shiro, M. Shionoya, *J. Am. Chem. Soc.* **2002**, *124*, 12494–12498.

[7] a) G. H. Clever, S. J. Reitmeier, T. Carell, O. Schiemann, *Angew. Chem.* **2010**, *122*, 5047–5049; *Angew. Chem. Int. Ed.* **2010**, *49*, 4927–4929; b) G. H. Clever, T. Carell, *Angew. Chem.* **2007**, *119*, 254–257; *Angew. Chem. Int. Ed.* **2007**, *46*, 250–253; c) G. H. Clever, Y. Söltl, H. Burks, W. Spahl, T. Carell, *Chem. Eur. J.* **2006**, *12*, 8708–8718; d) G. H. Clever, K. Polborn, T. Carell, *Angew. Chem.* **2005**, *117*, 7370–7374; *Angew. Chem. Int. Ed.* **2005**, *44*, 7204–7208.

[8] a) B. D. Heuberger, D. Shin, C. Switzer, *Org. Lett.* **2008**, *10*, 1091–1094; b) D. Shin, C. Switzer, *Chem. Commun.* **2007**, 4401–4403; c) C. Switzer, D. Shin, *Chem. Commun.* **2005**, 1342–1344; d) C. Switzer, S. Sinha, P. H. Kim, B. D. Heuberger, *Angew. Chem.* **2005**, *117*, 1553–1556; *Angew. Chem. Int. Ed.* **2005**, *44*, 1529–1532.

[9] a) L. Zhang, E. Meggers, *J. Am. Chem. Soc.* **2005**, *127*, 74–75; b) N. Zimmermann, E. Meggers, P. G. Schultz, *Bioorg. Chem.* **2004**, *32*, 13–25; c) N. Zimmermann, E. Meggers, P. G. Schultz, *J. Am. Chem. Soc.* **2002**, *124*, 13684–13685; d) S. Atwell, E. Meggers, G. Spraggon, P. G. Schultz, *J. Am. Chem. Soc.* **2001**, *123*, 12364–12367; e) E. Meggers, P. L. Holland, W. B. Tolman, F. E. Romesberg, P. G. Schultz, *J. Am. Chem. Soc.* **2000**, *122*, 10714–10715.

[10] a) H. Torigoe, A. Ono, T. Kozasa, *Chem. Eur. J.* **2010**, *16*, 13218–13225; b) I. Okamoto, K. Iwamoto, Y. Watanabe, Y. Miyake, A. Ono, *Angew. Chem.* **2009**, *121*, 1676–1679; *Angew. Chem. Int. Ed.* **2009**, *48*, 1648–1651; c) A. Ono, S. Cao, H. Togashi, M. Tashiro, T. Fujimoto, T. Machinami, S. Oda, Y. Miyake, I. Okamoto, Y. Tanaka, *Chem. Commun.* **2008**, 4825–4827; d) Y. Tanaka, S. Oda, H. Yamaguchi, Y. Kondo, C. Kojima, A. Ono, *J. Am. Chem. Soc.* **2007**, *129*, 244–245; e) Y. Miyake, H. Togashi, M. Tashiro, H. Yamaguchi, S. Oda, M. Kudo, Y. Tanaka, Y. Kondo, R. Sawa, T. Fujimoto, T. Machinami, A. Ono, *J. Am. Chem. Soc.* **2006**, *128*, 2172–2173; f) A. Ono, H. Togashi, *Angew. Chem.* **2004**, *116*, 4400–4402; *Angew. Chem. Int. Ed.* **2004**, *43*, 4300–4302.

[11] K. Tanaka, G. H. Clever, Y. Takezawa, Y. Yamada, C. Kaul, M. Shionoya, T. Carell, *Nat. Nanotechnol.* **2006**, *1*, 190–194.

[12] S. Johannsen, S. Paulus, N. Düpre, J. Müller, R. K. O. Sigel, *J. Inorg. Biochem.* **2008**, *102*, 1141–1151.

[13] a) R. M. Franzini, R. M. Watson, G. K. Patra, R. M. Breece, D. L. Tierney, M. P. Hendrich, C. Achim, *Inorg. Chem.* **2006**, *45*, 9798–9811; b) R. M. Watson, Y. A. Skorik, G. K. Patra, C. Achim, *J. Am. Chem. Soc.* **2005**, *127*, 14628–14639; c) D.-L. Popescu, T. J. Parolin, C. Achim, *J. Am. Chem. Soc.* **2003**, *125*, 6354–6355; d) A. Küsel, J. Zhang, M. Alvariño Gil, A. C. Stückl, W. Meyer-Klaucke, F. Meyer, U. Diedrichsen, *Eur. J. Inorg. Chem.* **2005**, 4317–4324; e) K. Ohr, R. L. McLaughlin, M. E. Williams, *Inorg. Chem.* **2007**, *46*, 965–974; f) B. P. Gilmartin, K. Ohr, R. L. McLaughlin, R. Koerner, M. E. Williams, *J. Am. Chem. Soc.* **2005**, *127*, 9546–9555.

[14] a) M. K. Schlegel, L. Zhang, N. Pagano, E. Meggers, *Org. Biomol. Chem.* **2009**, *7*, 476–482; b) M. K. Schlegel, L.-O. Essen, E. Meggers, *J. Am. Chem. Soc.* **2008**, *130*, 8158–8159.

[15] a) T. Ihara, T. Ishii, N. Araki, A. W. Wilson, A. Jyo, *J. Am. Chem. Soc.* **2009**, *131*, 3826–3827; b) M. G. Santangelo, P. M. Antoni, B. Spingler, G. Jeschke, *ChemPhysChem* **2010**, *11*, 599–606.

[16] F. Seela, T. Wenzel, *Helv. Chim. Acta* **1994**, *77*, 1485–1499.

[17] F. Seela, T. Wenzel, *Helv. Chim. Acta* **1995**, *78*, 833–846.

[18] V. Milata, J. Saloň, *Org. Prep. Proced. Int.* **1999**, *31*, 347–348.

[19] T. A. Devlin, D. J. Jebaratnam, *Synth. Commun.* **1995**, *25*, 711–718.

[20] E. Cubero, N. G. A. Abrescia, J. A. Subirana, F. J. Luque, M. Orozco, *J. Am. Chem. Soc.* **2003**, *125*, 14603–14612.

[21] D. M. Gray, R. L. Ratliff, M. R. Vaughan, *Methods Enzymol.* **1992**, *211*, 389–406.

[22] L. E. Kapinos, A. Holý, J. Günter, H. Sigel, *Inorg. Chem.* **2001**, *40*, 2500–2508.

[23] a) N. G. A. Abrescia, C. González, C. Gouyette, J. A. Subirana, *Biochemistry* **2004**, *43*, 4092–4100; b) G. Raghunathan, H. T. Miles, V. Sasisekharan, *Biopolymers* **1994**, *34*, 1573–1581.

[24] a) P. Wu, B. S. Fujimoto, J. M. Schurr, *Biopolymers* **1987**, *26*, 1463–1488; b) B. S. Fujimoto, J. M. Miller, N. S. Ribeiro, J. M. Schurr, *Biophys. J.* **1994**, *67*, 304–308.

[25] H. M. Berman, B. Schneider, in *Oxford Handbook of Nucleic Acid Structure* (Ed.: S. Neidle), Oxford University Press, Oxford, **1999**, pp. 295–312.

[26] N. Morgner, T. Kleinschroth, H.-D. Barth, B. Ludwig, B. Brutschy, *J. Am. Soc. Mass Spectrom.* **2007**, *18*, 1429–1438.

[27] J. Hoffmann, T. L. Schmidt, A. Heckel, B. Brutschy, *Rapid Commun. Mass Spectrom.* **2009**, *23*, 2176–2180.

[28] A. Bondi, *J. Phys. Chem.* **1964**, *68*, 441–451.
[29] a) P. Pyykkö, *Chem. Rev.* **1997**, *97*, 597–636; b) P. D. Harvey, M. Drouin, A. Michel, D. Perreault, *J. Chem. Soc. Dalton Trans.* **1993**, 1365–1369.
[30] C. Fonseca Guerra, F. M. Bickelhaupt, J. G. Snijders, E. J. Baerends, *Chem. Eur. J.* **1999**, *5*, 3581–3594.
[31] a) F. M. Bickelhaupt, E. J. Baerends, *Rev. Comput. Chem.* **2000**, *15*, 1–86; b) C. Fonseca Guerra, J.-W. Handgraaf, E. J. Baerends, F. M. Bickelhaupt, *J. Comput. Chem.* **2004**, *25*, 189–210.
[32] S. S. Mallajosyula, S. K. Pati, *Angew. Chem.* **2009**, *121*, 5077–5081; *Angew. Chem. Int. Ed.* **2009**, *48*, 4977–4981.
[33] N. Morgner, H.-D. Barth, B. Brutschy, *Austr. J. Chem.* **2006**, *59*, 109–114.
[34] a) G. te Velde, F. M. Bickelhaupt, E. J. Baerends, C. Fonseca Guerra, S. J. A. van Gisbergen, J. G. Snijders, T. Ziegler, *J. Comput. Chem.* **2001**, *22*, 931–967; b) C. Fonseca Guerra, J. G. Snijders, G. te Velde, E. J. Baerends, *Theor. Chem. Acc.* **1998**, *99*, 391–403; c) ADF2009.01, SCM, Theoretical Chemistry, Vrije Universiteit, Amsterdam, The Netherlands, http://www.scm.com/.
[35] a) S. Grimme, *J. Comput. Chem.* **2004**, *25*, 1463–1473; b) S. Grimme, *J. Comput. Chem.* **2006**, *27*, 1787–1799; c) A. D. Becke, *Phys. Rev. A* **1988**, *38*, 3098–3100; d) C. Lee, W. Yang, R. G. Parr, *Phys. Rev. B* **1988**, *37*, 785–789.
[36] a) C. Fonseca Guerra, T. van der Wijst, J. Poater, M. Swart, F. M. Bickelhaupt, *Theor. Chem. Acc.* **2010**, *125*, 245–252; b) C. Fonseca Guerra, F. M. Bickelhaupt, J. G. Snijders, E. J. Baerends, *J. Am. Chem. Soc.* **2000**, *122*, 4117–4128.
[37] J. G. Snijders, P. Vernooijs, E. J. Baerends, *At. Data Nucl. Tables* **1981**, *26*, 483–509.
[38] E. van Lenthe, E. J. Baerends, J. G. Snijders, *J. Chem. Phys.* **1994**, *101*, 9783–9792.
[39] a) A. Klamt, *J. Phys. Chem.* **1995**, *99*, 2224–2235; b) A. Klamt, G. Schüürmann, *J. Chem. Soc. Perkin Trans. 2* **1993**, 799–805; c) C. C. Pye, T. Ziegler, *Theor. Chem. Acc.* **1999**, *101*, 396–408.
[40] Y. Marcus, *J. Chem. Soc. Faraday Trans.* **1991**, *87*, 2995–2999.

Received: October 12, 2010
Revised: February 12, 2011
Published online: May 5, 2011

